Localized interfacial Phonon Modes at the Electronic Axion Domain Wall

Abhinava Chatterjee, Mourad Oudich, Yun Jing, Chao-Xing Liu

▶ **To cite this version:**

Abhinava Chatterjee, Mourad Oudich, Yun Jing, Chao-Xing Liu. Localized interfacial Phonon Modes at the Electronic Axion Domain Wall. Physical Review B, 2024, 110 (16), pp.L161301. ⟨10.1103/PhysRevB.110.L161301⟩. ⟨hal-04795950⟩

HAL Id: hal-04795950

https://hal.science/hal-04795950v1

Submitted on 21 Nov 2024

HAL is a multi-disciplinary open access archive for the deposit and dissemination of scientific research documents, whether they are published or not. The documents may come from teaching and research institutions in France or abroad, or from public or private research centers.

L'archive ouverte pluridisciplinaire **HAL**, est destinée au dépôt et à la diffusion de documents scientifiques de niveau recherche, publiés ou non, émanant des établissements d'enseignement et de recherche français ou étrangers, des laboratoires publics ou privés.

HAL Authorization

Localized interfacial Phonon Modes at the Electronic Axion Domain Wall

Abhinava Chatterjee[1], Mourad Oudich[2,3], Yun Jing[2], and Chao-Xing Liu*[1]

[1] *Department of Physics, The Pennsylvania State University, University Park, Pennsylvania 16802, USA*
[2] *Graduate Program in Acoustics, The Pennsylvania State University, University Park, Pennsylvania 16802, USA*
[3] *Université de Lorraine, CNRS, Institut Jean Lamour, F-54000 Nancy, France*

The most salient feature of electronic topological states of matter is the existence of exotic electronic modes localized at the surface or interface of a sample. In this work, in an electronic topological systems, we demonstrate the existence of localized phonon modes at the domain wall between topologically trivial and non-trivial regions, in addition to the localized interfacial electronic states. In particular, we consider a theoretical model for the Dirac semimetal with a gap opened by external strains and study the phonon dynamics, which couples to electronic degrees of freedom via strong electron-phonon interaction. By treating the phonon modes as pseudo-gauge fields, we find that the axion type of terms for phonon dynamics can emerge in gapped Dirac semimetal model and lead to interfacial phonon modes localized at the domain wall between trivial and non-trivial regimes that possess the axion parameters 0 and π, respectively. We also discuss the physical properties and possible experimental probe of such interfacial phonon modes.

Introduction - At the surface of a topological electronic material or at the domain wall between two topologically distinct regions, surface or interfacial electronic modes can emerge and exhibit exotic physical phenomena [1–4]. The existence of these surface/interfacial electronic modes is a direct consequence on non-trivial topology of the bulk electronic band structure in topological materials, a general feature summarized as the bulk–boundary correspondence [5–11]. The connection between bulk topological states and the corresponding boundary modes is not limited to electronic states, but has also been generalized to other physical systems, including photonics [12–15], phononics [16–18], magnonics [19, 20], electric circuits [21, 22], and mechanical systems [23–25], in which a variety of boundary modes have been identified and classified, and many of them have been experimentally observed.

Our current understanding and classification of topological states and boundary modes (e.g. electrons, phonons, magnons, *etc*,) is mainly limited to systems with one type of quasi-particles. As the interaction between different quasi-particles, e.g. electron-phonon interaction, generally exists in realistic materials [26–31], one may ask if topological states and the boundary modes of different quasi-particles are connected to each other. Topological polariton [32–37] provides such an example. Here we wonder, in a system with strong electron-phonon interaction, if a boundary phonon mode can exist for a topologically non-trivial electronic system.

In this work, we give an affirmative answer to this question and show that an interfacial phonon mode can exist at the domain wall between two topologically distinct regions with different electronic axion parameters. Particularly, we consider the Dirac semimetal model with a small gap controlled by external static strain serving as effective axion fields. Acoustic phonon dynamics is strongly influenced by the axion term through electron-acoustic-phonon (or equivalently electron-strain) interaction, which gives rise to interfacial phonon modes localized at the domain wall between topologically trivial and non-trivial regions of electronic states.

Electron-acoustic-phonon Interaction and Valley Axion Field in Gapped Dirac Semimetals - We consider three-dimensional (3D) Dirac semimetal, e.g. Na_3Bi [38, 39], with electron-phonon coupling, described by the Hamiltonian $H = H_e + H_{e-ph}$. H_e is the model Hamiltonian for 3D Dirac semimetals [40, 41], and its detailed form is described in Sec. S1 B of Supplementary Materials (SM) [42]. The crystal symmetry of H_e is described by the D_{6h} group that can be generated by six-fold rotation $\hat{C}_{6z}$, inversion $\hat{I}$ and two-fold rotation $\hat{C}_{2x}$. The conduction and valence bands of H_e have the crossings located at the momenta $\mathbf{K}_a = (0, 0, ak_c)$ with $a = \pm$ and k_c depending on material parameters. Around these crossing points, the effective Hamiltonians behave as 3D massless Dirac fermions with nodes protected by $\hat{C}_{6z}$, as schematically depicted in Fig. 1(a)(i). The index $a = \pm$ in $\mathbf{K}_a$ is regarded as two "valleys" that are related by time reversal $\hat{T}$. For electron-phonon interaction H_{e-ph}, we consider acoustic phonons that can be described by the strain tensor $u_{ij} = \frac{1}{2}(\partial_i u_j + \partial_j u_i)$ $(i, j = x, y, z)$ with the displacement field $\mathbf{u}$ [43]. Based on the D_{6h} group for Na_3Bi, we can construct all the terms up to the linear orders in both the momentum $\mathbf{k}$ and strain tensor u_{ij} (Sec. S1 B of SM [42]).

We next project the total Hamiltonian H into the subspace spanned by the massless Dirac fermions at $\mathbf{K}_a$, and the corresponding effective Hamiltonian is written as $H_{eff} = \sum_{a=\pm} H_{eff,a}$ with $H_{eff,a}$ given by

$$\begin{aligned} H_{eff,a} = {} & A_0^{pse}\mathbb{I} + A_0\pi_x\Gamma_3 - A_0\pi_y\Gamma_4 - 2M_1k_c\pi_z\Gamma_5 \\ & + |m|\left(\cos\Phi_a\Gamma_1 - \sin\Phi_a\Gamma_2\right). \end{aligned} \tag{1}$$

Here the Γ matrices are $\Gamma_i = \sigma_i \otimes \tau_1, \Gamma_4 = I \otimes \tau_2, \Gamma_5 = I\otimes\tau_3, \Gamma_{ij} = \epsilon_{ijk}\sigma_k\otimes I, \Gamma_{i4} = \sigma_i\otimes\tau_3, \Gamma_{i5} = -\sigma_i\otimes\tau_2, \Gamma_{45} = I \otimes \tau_1$ with $i, j = 1, 2, 3$. I labels the identity matrix and σ, τ are two sets of Pauli matrices representing spin and orbital degrees of freedoms, respectively. $\boldsymbol{\pi} = \mathbf{k} - \mathbf{A}_a^{pse}$ with the pseudo-gauge field [44–47] $A_0^{pse} = \tilde{C}(\{u_{ij}\})$

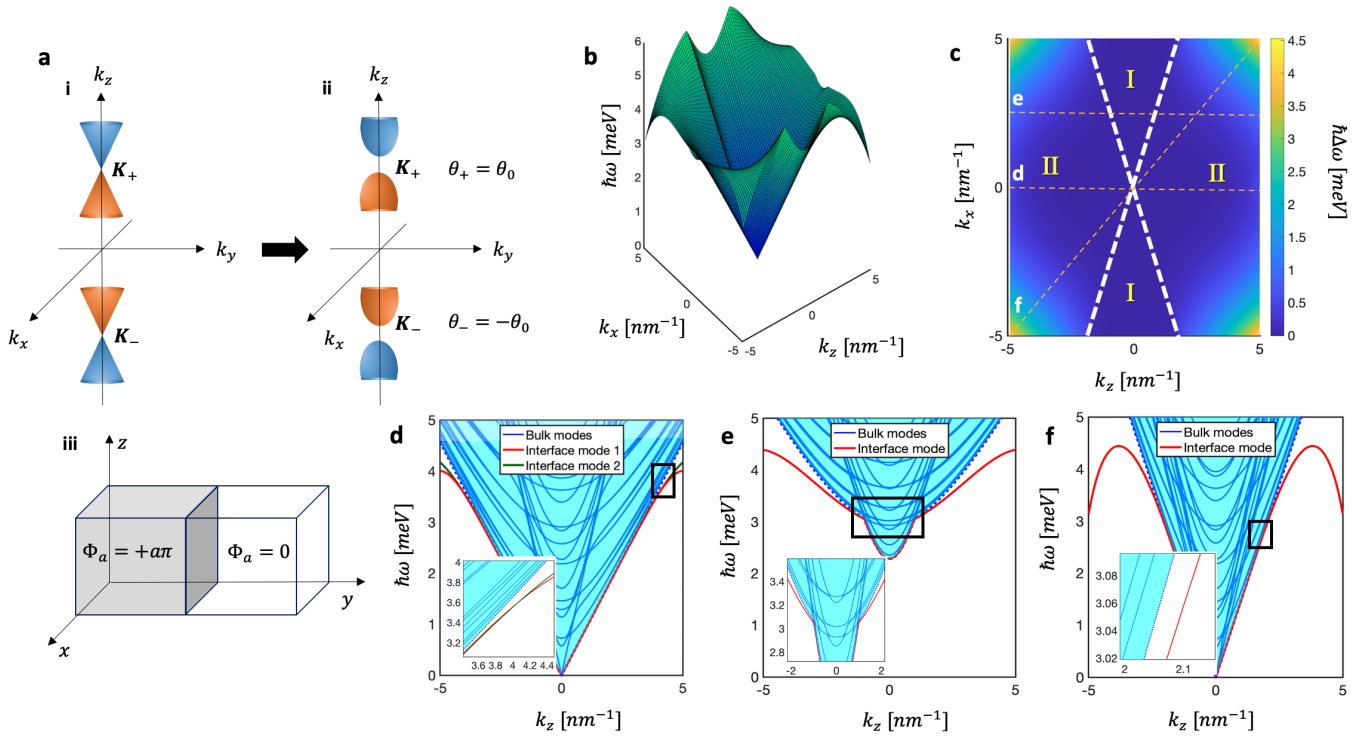

FIG. 1. (a) Setup. (i) The spectrum for Na_3Bi is gapless at the $K_\pm$ points. (ii) The external strain leads to a gap in the spectrum where $\theta_0 = \pi/2$ by choosing the static strain $u^0_{xy} \to 0$ and $u^0_{xx} - u^0_{yy} \neq 0$. (iii) The variation of the static axion angle along the y direction which induces a domain wall at the interface. (b) Interface mode dispersion $\hbar\omega$ as a function of in-plane momenta (k_x, k_z). (c) Energy difference between the lowest bulk mode and the next lowest mode $\hbar\Delta\omega = \hbar(\omega_2 - \omega_1)$. The thick white dashed lines separate Region I where the interface mode merges with the bulk modes, and Region II where the interfacial mode is below the bulk modes in energy. The thin dashed orange lines show cuts in the $k_x k_z$ plane for which we have plotted the energy dispersion in (d), (e), and (f). (d) Band dispersion at $k_x = 0$ where two interface modes (marked in red and green lines) exist. The bulk modes are highlighted in blue and shaded with a cyan region. Inset: the band crossing between the two interface modes. (e) Band dispersion at $k_x = 2.5\,\mathrm{nm}^{-1}$ where one interface mode (red line) merges into the bulk modes for $k_z \sim [-1, 1]\,\mathrm{nm}^{-1}$ (Inset),consistent with Region I of (c). (f) Band dispersion at $k_x = k_z$ where one interface mode (red) exists. Inset: the interface mode's velocity is than that of the the bulk modes. The lowest bulk mode is shown with the dotted blue line in (d)-(f). We use $r = .8$; $s = .713$; $t = .9$ in units of $10^{-12} m^4/s^2$ and $a = 6.75, b = 3.17, c = 1.01, d = 1.93, f = 11.02$ in units of $10^6\,\mathrm{m}^2/\mathrm{s}^2$.

and $\mathbf{A}^{pse}_a = a\left[-A_4 k_c u_{xz}, A_4 k_c u_{yz}, \tilde{M}(\{u_{ij}\})\right]$ $(a = \pm)$. $\tilde{C}(\{u_{ij}\}) = C_3 u_{zz} + C_4(u_{xx} + u_{yy})$, $\tilde{M}(\{u_{ij}\}) = M_3 u_{zz} + M_4(u_{xx} + u_{yy})$, $|m| = Dk_c\sqrt{(2u_{xy})^2 + (u_{xx} - u_{yy})^2}$, $\Phi_a = a\theta$, $\cot\theta = \frac{u_{xx}-u_{yy}}{2u_{xy}}$, with $C_{3,4}, M_{3,4}, A_{0,4}, D$ as material parameters that are constant over the whole system [42]. $|m|\,(\cos\Phi_a\Gamma_1 - \sin\Phi_a\Gamma_2)$ is a complex valley dependent mass term due to strain that can gap out the Dirac points, as depicted in Fig. 1(a) (ii). We consider a static strain $u^{(0)}_{ij}$ and a dynamical strain field δu_{ij}, $u_{ij} = u^{(0)}_{ij} + \delta u_{ij}$, in which the static strain can be nonuniform and is chosen only to possess non-zero $u^{(0)}_{xx} - u^{(0)}_{yy}$ and $u^{(0)}_{xy}$ while all other components are zero. Consequently, $u^{(0)}_{ij}$ can produce the Φ_a field but not $\mathcal{A}^{pse} = (A^{pse}_0, \mathbf{A}^{pse}_a)$. We consider acoustic phonons that create a dynamical strain field δu_{ij}, leading to the $\mathcal{A}^{pse}$ field. A^{pse}_0 has the same sign for both valleys, while $\mathbf{A}^{pse}_a$ flips its sign between two valleys, as required by $\hat{T}$.

With the Fermi energy within the energy gap of the effective Hamiltonian Eq.1, we can integrate out the Dirac fermions and obtain the effective action for $\mathcal{A}^{pse}$ as[48]

$$S_{ax} = \textstyle\sum_{a=\pm} S_{eff,a},$$
$$S_{eff,a} = \frac{1}{32\pi^2}\int dtd^3r\,\Phi_a\epsilon^{\mu\nu\rho\delta}F_{\mu\nu,a}F_{\rho\delta,a}, \qquad (2)$$

where $F_{\mu\nu,a} = \partial_\mu\mathcal{A}^{pse}_{\nu,a} - \partial_\nu\mathcal{A}^{pse}_{\mu,a}$ and $\mu, \nu = 0, 1, 2, 3$. $S_{eff,a}$ has a similar form as the axion electrodynamics [49–51], but it is for the $\mathcal{A}^{pse}$ field connected to the strain field. Thus, $S_{eff,a}$ is expected to influence phonon dynamics. Due to $\hat{T}$, the Φ_a field has opposite signs for two valleys, and thus we dub Φ_a as the "valley axion field". The derivation for the explicit form of S_{ax} can be found in Sec. S1 C of SM [42]. S_{ax} is invariant under $\hat{C}_{6z}$, $\hat{C}_{2x}$, $\hat{T}$ and $\hat{I}$. We can re-write the effective action in a compact form

$$S_{ax} = -\int dtd^3r\,(\nabla\theta\cdot\mathbf{h}), \qquad (3)$$

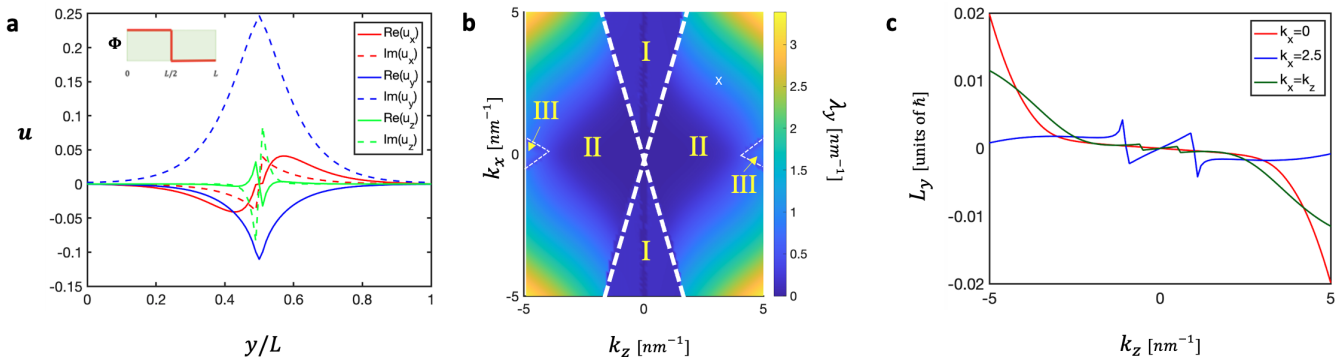

FIG. 2. (a) The spatial distribution of the real and imaginary parts of the displacement field of the interface phonon mode at point X where $(k_x, k_z) = (2.5, 3)nm^{-1}$. The u_y component (both real and imaginary) is even across the axion domain wall whereas the x and z components are odd. (b) The inverse decay length (Λ) of the dominant u_y component of the displacement as a function of (k_x, k_z) (c) The out of plane (y direction) phonon angular momentum of the interface mode at $k_x = 0$ (red) , $k_x = 2.5nm^{-1}$ (blue) and $k_x = k_z$ (dark green). We use $r = .8$; $s = .713$; $t = .9$ in units of $10^{-12}m^4/s^2$ and $a = 6.75, b = 3.17, c = 1.01, d = 1.93, f = 11.02$ in units of $10^6 m^2/s^2$.

where $h_x = -\tilde{C}\left(A_0A_4M_0\partial_z u_{yz} + A_0^2\partial_y\tilde{M}\right)$, $h_y = \tilde{C}\left(A_0A_4M_0\partial_z u_{xz} + A_0^2\partial_x\tilde{M}\right)$ and $h_z = A_0A_4M_0\tilde{C}\left(\partial_x u_{yz} - \partial_y u_{xz}\right)$. S_{ax} vanishes when θ is a constant and is non-zero at the θ domain wall.

Interficial Phonon Modes at Axion Domain Wall- From the functional derivative $\delta(S_0+S_{ax})/\delta\mathbf{u} = 0$, where S_0 is the bulk elastic action for the D_{6h} group with 5 independent elastic modulii a, b, c, d, f [52, 53] and S_{ax} is the axion term in Eq. (2), one can derive the equation of motion for the phonon displacement field $\mathbf{u}$ as

$$H_{ph}\mathbf{u} = \rho\omega^2\mathbf{u}, \tag{4}$$

where ρ is mass density, ω is phonon frequency and H_{ph} is the effective phonon Hamiltonian given by $H_{ph} = H_{bulk} + H_{ax}$ (Sec. S1 F and Sec. S2 A of SM [42]). Here we assume the translation symmetry along the x and z directions, so that the in-plane momentum $\mathbf{k}_\parallel = (k_x, k_z)$ a good quantum number. Along the y direction, we consider a domain wall configuration for the axion field, $\Phi_a = a\theta(y) = a\pi\Theta(L/2 - y)$, where $\Theta(y)$ is the step function, $a = \pm$ and L is the system size as depicted in In Fig. 1(a) (iii). This Φ configuration can be achieved by applying a nonuniform static strain $u^{(0)}_{xx} - u^{(0)}_{yy} < 0$ for $y < L/2$ and $u^{(0)}_{xx} - u^{(0)}_{yy} > 0$ for $y > L/2$ in the limit $u^{(0)}_{xy} \to 0$. Since $\Delta\Phi = \pi$, the interface is an electronic axion domain wall. By choosing the wave-function ansatz $\mathbf{u}(\mathbf{r}, t) = \mathbf{f}(y)e^{i\mathbf{k}_\parallel\cdot\mathbf{r}_\parallel}$ with $\mathbf{r}_\parallel = (x, z)$ and $\mathbf{k}_\parallel = (k_x, k_z)$, the form of the Hamiltonian H_{ax} is given by (Sec. S2 A of SM [42])

$$H_{ax} = \begin{pmatrix} 0 & \frac{s}{2}k_z^2\{\partial_y, \frac{\partial\theta}{\partial y}\} & i\frac{\partial\theta}{\partial y}\alpha(k_x, k_z) \\ -\frac{s}{2}k_z^2\{\partial_y, \frac{\partial\theta}{\partial y}\} & 0 & -\frac{1}{2}(s+t)k_xk_z\{\partial_y, \frac{\partial\theta}{\partial y}\} \\ -i\frac{\partial\theta}{\partial y}\alpha(k_x, k_z) & +\frac{1}{2}(s+t)k_xk_z\{\partial_y, \frac{\partial\theta}{\partial y}\} & 0 \end{pmatrix}, \tag{5}$$

where $\alpha(k_x, k_z) = rk_z^3 - (s+t)k_x^2k_z$, $\frac{\theta_0}{2\pi^2 Z}\frac{J}{2}C_3 \equiv r$, $\frac{\theta_0}{2\pi^2 Z}\frac{J}{2}C_4 \equiv s$ and $\frac{\theta_0}{2\pi^2 Z}A_0^2(C_3M_4 - C_4M_3) \equiv t$ with $J = -2A_0A_4M_0$ and $Z = 2A_0^2M_1k_c$. H_{ax} contains $\frac{\partial\theta}{\partial y}$, which is only non-zero at the axion domain wall.

We numerically solve H_{ph} (Sec. S3 in SM [42]). Fig. 1(b) illustrates the anisotropic dispersion of the lowest frequency phonon mode in the $\mathbf{k}_\parallel$ plane. Fig. 1(d) and (e) show the phonon dispersion along the k_z direction for $k_x = 0$ and $k_x = 2.5nm^{-1}$, respectively, while Fig. 1(f) is for phonon dispersion along the $k_x = k_z$ direction. The cyan shaded areas in Fig. 1(d)-(f) represent the dispersion of bulk phonons that can be obtained from the eigen-frequency of H_{bulk}. In the insets of Fig. 1(d)-(f), additional phonon modes emerge with their frequency below the bulk phonon frequency. We find one mode (red) in Fig. 1(e) and (f), and two modes (red and green) in Fig. 1(d). Fig. 1(c) depicts the frequency difference between the lowest bulk phonon frequency and the lowest phonon modes in the domain wall configuration in the $\mathbf{k}_\parallel$ space, which can be divided into two regions. This frequency difference is zero in Region I, while it becomes positive in Region II, implying the existence of the modes with their frequencies below bulk phonon frequency. To further demonstrate their origin

from the axion domain wall, the wave function $\mathbf{f}(y)$ for the y-directional distribution of the displacement field at $X = (k_x, k_z) = (2.5, 3)nm^{-1}$ is depicted in Fig. 2(a). All components of displacement field $\mathbf{u}$ decay exponentially away form the the axion domain wall located at $y = L/2$, thus unambiguously demonstrating the interfacial nature of these phonon modes. The interfacial phonon wave functions $\mathbf{f}(y)$ for different momenta are further discussed in Fig. S3 of SM [42]. We can use the exponential function $\sim e^{-\lambda_y|y-L/2|}$ to fit to the solution $f_y(y)$ that exhibits the largest amplitude for different $\mathbf{k}_\parallel$, and the λ_y parameter that represents the inverse of localization length is shown as a function of $\mathbf{k}_\parallel$ in Fig. 2(b). $\lambda_y = 0$ in Region I and nonzero λ_y appears in Region II and III, which means the interfacial modes only exist in Regions II and III, consistent with Fig. 1(c). Region II has one interfacial mode while Region III contains two interfacial modes. More information on these two interfacial modes can be found in Fig. S7 of SM [42]. With increasing $|\mathbf{k}_\parallel|$, λ_y increases, and the localization length decreases. Thus, the interfacial phonon modes become more localized for a large momentum. The existence of the interfacial phonon modes can be understood by analytically solving the eigen-equation (4) with the domain wall configuration under certain approximations. Two analytically solvable cases are considered in Sec. S2 B,D of SM [42], and *Case I* shows the presence of interfacial modes with non-zero angular momentum, whereas *Case II* shows the presence of two interface modes, similar to the case in Fig. 1(d). Below we will only focus on *Case I* while *Case II* is discussed in Sec. S2 D of SM [42].

For *Case I*, we choose $r \neq 0$ and $s = t = 0$, such that only $\alpha = rk_z^3 \neq 0$ and take the isotropic approximation for H_{bulk} with $a = c_l^2 - c_t^2, b = d = c_t^2, c = c_l^2 - 2c_t^2, f = c_l^2$. We further assume $c_t = c_l = c_0$ (the exact form of the Hamiltonian is discussed in Eqs(58,59) of Sec. S2 B of SM [42]). Due to the $\delta(y)$-function, we look for exponentially localized phonon modes around $y = 0$ with the ansatz $\mathbf{u} = \sum_{\tau=1}^{3} A_\tau e^{-\lambda_\tau y}\mathbf{u}_0^\tau(y, \lambda_\tau)$ for $y > 0$ and $\mathbf{u} = \sum_{\tau=1}^{3} B_\tau e^{\xi_\tau y}\mathbf{v}_0^\tau(y, \lambda_\tau)$ for $y < 0$, where λ_τ and ξ_τ are the inverse localization lengths of mode τ for $y > 0$ and $y < 0$ respectively. $\mathbf{u}_0$ and $\mathbf{v}_0$ are the eigenmodes for $y > 0$ and $y < 0$, respectively. By matching the wave functions at the boundary $y = 0$, we obtain 6 linear equations for the variables $A_{1,2,3}$ and $B_{1,2,3}$. By solving for the characteristic equation, we find bulk modes with $\omega = c_0 k$ ($k = \sqrt{k_x^2 + k_z^2}$) and an interfacial mode with $\omega = \left[(c_0 k)^2 - (\alpha(k_x, k_z)/c_0)^2\right]^{1/2}$. The eigen-vector of the interfacial phonon mode is $\mathbf{u} = Ne^{-\lambda|y|}(\mathrm{sgn}(\alpha), 0, -i)^T$ with the normalization factor N and the inverse localization length $\lambda = |\alpha(k_x, k_z)|/c_0^2$. The existence of the localized interfacial phonon mode can also be understood from the Jackiw-Rebbi-like mechanism [54, 55]. In contrast to Ref. [55], where the localized mode is a zero energy mode resulting from the spatially varying coefficient of the kinetic energy term, which contains the domain wall structure, for a scalar field, the localized interfacial phonon mode in our work has a finite frequency and is obtained from higher-order-momentum term in the effective action of phonons, which is a consequence of electron-phonon interactions (see Sec. S2 C of SM [42] for details. This interfacial phonon mode is circularly polarized and the corresponding phonon angular momentum, defined by $l_i = \hbar \mathbf{u}_0^\dagger M_i \mathbf{u}_0$ where $i = x, y, z$ and $(M_i)_{jk} = (-i)\epsilon_{ijk}$ [56, 57], has non-zero y-component, $l_y = \hbar\mathrm{sgn}(\alpha) = \hbar\mathrm{sgn}(k_z)$. The quantized angular momentum l_y is a consequence of the isotropic approximation. For a more realistic situation, we numerically evaluate the angular momentum of the interfacial phonon modes in Fig. 2(c), in which l_y strongly depends on k_z and increases rapidly for a large k_z. l_y changes its sign for opposite momentum k_z and thus reveals a helical nature as required by $\hat{T}$ [58, 59]. More information of phonon angular momentum is provided in Fig. S5, and discussed in Sec. S5 of SM [42]. This phonon helicity can be probed via temperature gradient induced phonon angular momentum [57–60]. Our numerical and symmetry analysis suggests that the z-directional temperature gradient can induce the y-directional angular momentum l_y via the axion term, and this response is absent if there is no axion term, as discussed in Sec. S5 B,C of SM (Fig. S11b) [42]. With increasing $|\mathbf{k}_\parallel|$, the dispersion of the interfacial phonon mode generally exhibits a maximum at a certain momentum and then its frequency drops down. With further increasing $|\mathbf{k}_\parallel|$, the phonon frequency can drop to zero and then become imaginary, implying a lattice instability. Nevertheless, our effective action of acoustic phonon dynamics is only valid for the momentum within the first Brillouin zone and breaks down closer to the Brillouin zone boundary (roughly at $\sim 10nm^{-1}$), so we restrict our in-plane momenta to be $5nm^{-1}$. Within this momentum range, we find the axion term H_{ax} is not strong enough for a lattice instability. A surface acoustic wave can generally exist at the surface of an elastic material (described by the phonon Hamiltonian H_{bulk} with a stress-free boundary condition), even in the absence of the valley axion term [43]. The presence of axion term will also strongly modify the surface acoustic wave (Sec. S4 of SM [42]).

Conclusion - In this work, we demonstrate the existence of the interfacial phonon modes localized at the domain wall between two regions with different valley axion parameters due to the electron-phonon interaction in the gapped Dirac semimetal model. Although our model is derived for Na_3Bi, this mechanism can be generalized to other Dirac materials. The key requirement is that the low-energy Dirac Hamiltonian should be located at generic momenta that are not $\hat{T}$-invariant, as the complex mass and the pseudo-gauge field terms in Eq. (1) generally break $\hat{T}$. Given this requirement, the existing Dirac materials, Na_3Bi and Cd_3As_2 [40, 41], may host interfacial phonon modes from our mechanism, which may be probed via different experimental methods. We notice that the interfacial phonon modes have been previously observed in epitaxial Si-Ge interface via a combi-

nation of Raman spectroscopy and high-energy- resolution electron energy-loss spectroscopy (EELS) in a scanning transmission electron microscope [61], and in epitaxial cubic boron nitride/diamond heterointerface using 4D EELS [62]. The unique phonon angular momentum distribution in the momentum space [57–60] may help to distinguish this mechanism of interfacial phonon modes from other origins [61, 62]. Furthermore, phonon angular momentum may couple to external magnetic fields via Dirac electrons and potentially lead to a phonon thermal Hall effect [63–65]. Our mechanism can also be applied to magnetic topological materials, e.g. $MnBi_2Te_4$, even though the Dirac Hamiltonian is located at a high-symmetry momenta [66–68] but $\hat{T}$ is already broken by its intrinsic magnetism. One may also expect interfacial magnon mode in these magnetic topological materials due to electron-magnon interaction. Multiple interfacial modes of different quasiparticles (e.g. electrons, phonons, magnons, *etc*) may coexist at the same domain wall due to strong interactions.

Acknowledgement - We acknowledge helpful discussions with Z. Bi and N. Kalyanapuram. A.C. and C.-X.L. acknowledge support from NSF grant via the grant number DMR-2241327 and the ONR Award (N000142412133).

[1] X.-L. Qi and S.-C. Zhang, Topological insulators and superconductors, Reviews of Modern Physics **83**, 1057 (2011).
[2] M. Z. Hasan and C. L. Kane, Colloquium: topological insulators, Reviews of modern physics **82**, 3045 (2010).
[3] B. Yan and S.-C. Zhang, Topological materials, Reports on Progress in Physics **75**, 096501 (2012).
[4] B. J. Wieder, B. Bradlyn, J. Cano, Z. Wang, M. G. Vergniory, L. Elcoro, A. A. Soluyanov, C. Felser, T. Neupert, N. Regnault, *et al.*, Topological materials discovery from crystal symmetry, Nature Reviews Materials **7**, 196 (2022).
[5] S. Ryu and Y. Hatsugai, Topological origin of zero-energy edge states in particle-hole symmetric systems, Physical review letters **89**, 077002 (2002).
[6] A. P. Schnyder, S. Ryu, A. Furusaki, and A. W. Ludwig, Classification of topological insulators and superconductors in three spatial dimensions, Physical Review B **78**, 195125 (2008).
[7] R. S. Mong and V. Shivamoggi, Edge states and the bulk-boundary correspondence in dirac hamiltonians, Physical Review B **83**, 125109 (2011).
[8] S. Ryu, A. P. Schnyder, A. Furusaki, and A. W. Ludwig, Topological insulators and superconductors: tenfold way and dimensional hierarchy, New Journal of Physics **12**, 065010 (2010).
[9] Y. Tanaka, M. Sato, and N. Nagaosa, Symmetry and topology in superconductors–odd-frequency pairing and edge states–, Journal of the Physical Society of Japan **81**, 011013 (2011).
[10] A. Kitaev, Periodic table for topological insulators and superconductors, in *AIP conference proceedings*, Vol. 1134 (American Institute of Physics, 2009) pp. 22–30.
[11] Y. Hatsugai, Bulk-edge correspondence in graphene with/without magnetic field: Chiral symmetry, dirac fermions and edge states, Solid state communications **149**, 1061 (2009).
[12] L. Lu, J. D. Joannopoulos, and M. Soljačić, Topological photonics, Nature photonics **8**, 821 (2014).
[13] T. Ozawa, H. M. Price, A. Amo, N. Goldman, M. Hafezi, L. Lu, M. C. Rechtsman, D. Schuster, J. Simon, O. Zilberberg, *et al.*, Topological photonics, Reviews of Modern Physics **91**, 015006 (2019).
[14] J. Schulz, S. Vaidya, and C. Jörg, Topological photonics in 3d micro-printed systems. apl photon 6 (8): 080901 (2021).
[15] S. Vaidya, M. C. Rechtsman, and W. A. Benalcazar, Polarization and weak topology in chern insulators, Physical Review Letters **132**, 116602 (2024).
[16] Y. Liu, X. Chen, and Y. Xu, Topological phononics: from fundamental models to real materials, Advanced Functional Materials **30**, 1904784 (2020).
[17] H. Chen, W. Zhang, Q. Niu, and L. Zhang, Chiral phonons in two-dimensional materials, 2D Materials **6**, 012002 (2018).
[18] X.-Q. Chen, J. Liu, and J. Li, Topological phononic materials: Computation and data, The Innovation **2** (2021).
[19] F. Zhuo, J. Kang, A. Manchon, and Z. Cheng, Topological phases in magnonics, Advanced Physics Research , 2300054 (2023).
[20] P. A. McClarty, Topological magnons: A review, Annual Review of Condensed Matter Physics **13**, 171 (2022).
[21] E. J. Bergholtz, J. C. Budich, and F. K. Kunst, Exceptional topology of non-hermitian systems, Reviews of Modern Physics **93**, 015005 (2021).
[22] M. J. Gilbert, Topological electronics, Communications Physics **4**, 70 (2021).
[23] S. Zheng, G. Duan, and B. Xia, Progress in topological mechanics, Applied Sciences **12**, 1987 (2022).
[24] G. Ma, M. Xiao, and C. T. Chan, Topological phases in acoustic and mechanical systems, Nature Reviews Physics **1**, 281 (2019).
[25] X. Mao and T. C. Lubensky, Maxwell lattices and topological mechanics, Annual Review of Condensed Matter Physics **9**, 413 (2018).
[26] P. Thalmeier, Surface phonon propagation in topological insulators, Physical Review B **83**, 125314 (2011).
[27] S. Giraud and R. Egger, Electron-phonon scattering in topological insulators, Physical Review B **83**, 245322 (2011).
[28] S. Giraud, A. Kundu, and R. Egger, Electron-phonon scattering in topological insulator thin films, Physical Review B **85**, 035441 (2012).
[29] G. Huang, Surface lattice vibration and electron-phonon interaction in topological insulator bi2te3 (111) films from first principles, Europhysics Letters **100**, 17001 (2012).
[30] V. Parente, A. Tagliacozzo, F. Von Oppen, and F. Guinea, Electron-phonon interaction on the surface of a three-dimensional topological insulator, Physical Re-

view B **88**, 075432 (2013).
[31] I. Garate, Phonon-induced topological transitions and crossovers in dirac materials, Physical Review Letters **110**, 046402 (2013).
[32] T. Karzig, C.-E. Bardyn, N. H. Lindner, and G. Refael, Topological polaritons, Physical Review X **5**, 031001 (2015).
[33] W. Liu, Z. Ji, Y. Wang, G. Modi, M. Hwang, B. Zheng, V. J. Sorger, A. Pan, and R. Agarwal, Generation of helical topological exciton-polaritons, Science **370**, 600 (2020).
[34] S. Klembt, T. Harder, O. Egorov, K. Winkler, R. Ge, M. Bandres, M. Emmerling, L. Worschech, T. Liew, M. Segev, *et al.*, Exciton-polariton topological insulator, Nature **562**, 552 (2018).
[35] G. Hu, Q. Ou, G. Si, Y. Wu, J. Wu, Z. Dai, A. Krasnok, Y. Mazor, Q. Zhang, Q. Bao, *et al.*, Topological polaritons and photonic magic angles in twisted α-moo3 bilayers, Nature **582**, 209 (2020).
[36] M. Li, I. Sinev, F. Benimetskiy, T. Ivanova, E. Khestanova, S. Kiriushechkina, A. Vakulenko, S. Guddala, M. Skolnick, V. M. Menon, *et al.*, Experimental observation of topological z2 exciton-polaritons in transition metal dichalcogenide monolayers, Nature communications **12**, 4425 (2021).
[37] Y. V. Kartashov and D. V. Skryabin, Two-dimensional topological polariton laser, Physical review letters **122**, 083902 (2019).
[38] Z. Liu, B. Zhou, Y. Zhang, Z. Wang, H. Weng, D. Prabhakaran, S.-K. Mo, Z. Shen, Z. Fang, X. Dai, *et al.*, Discovery of a three-dimensional topological dirac semimetal, na3bi, Science **343**, 864 (2014).
[39] J. Xiong, S. K. Kushwaha, T. Liang, J. W. Krizan, M. Hirschberger, W. Wang, R. J. Cava, and N. P. Ong, Evidence for the chiral anomaly in the dirac semimetal na3bi, Science **350**, 413 (2015).
[40] Z. Wang, Y. Sun, X.-Q. Chen, C. Franchini, G. Xu, H. Weng, X. Dai, and Z. Fang, Dirac semimetal and topological phase transitions in a 3 bi (a= na, k, rb), Physical Review B **85**, 195320 (2012).
[41] Z. Wang, H. Weng, Q. Wu, X. Dai, and Z. Fang, Three-dimensional dirac semimetal and quantum transport in cd 3 as 2, Physical Review B **88**, 125427 (2013).
[42] See Supplementary Material at [URL]. In Sec. S1, we present the effective theory of Na_3Bi based on the symmetry properties of D_{6h} symmetry group with relevant material parameters. We derive the effective action S_{eff} and discuss the symmetry properties of S_{eff}. We close Sec. S1 with the bulk action and deriving the equation of motion in the presence of the axion term. In Sec. S2, we provide details of the analytical solutions for *Case I* and *Case II*. In Sec. S3, we provide the framework for our numerical calculations and elaborate on some of the numerical features presented in the main text. In Sec. S4, we perform detailed calculations to show the influence of the axion term on the already present surface modes of an elastic material with an open boundary. Lastly, in Sec. S5, we present the formalism for the phonon angular momentum and describe probing the helical nature of the interface phonon modes using a temperature gradient. The Supplementary Material also contains Refs. [69–74].
[43] L. D. Landau, E. M. Lifshitz, A. M. Kosevich, and L. P. Pitaevskii, *Theory of elasticity: volume 7*, Vol. 7 (Elsevier, 1986).
[44] F. de Juan, J. L. Manes, and M. A. Vozmediano, Gauge fields from strain in graphene, Physical Review B **87**, 165131 (2013).
[45] D. Pikulin, A. Chen, and M. Franz, Chiral anomaly from strain-induced gauge fields in dirac and weyl semimetals, Physical Review X **6**, 041021 (2016).
[46] R. Ilan, A. G. Grushin, and D. I. Pikulin, Pseudo-electromagnetic fields in 3d topological semimetals, Nature Reviews Physics **2**, 29 (2020).
[47] J. Yu and C.-X. Liu, Pseudo-gauge fields in dirac and weyl materials, in *Semiconductors and Semimetals*, Vol. 108 (Elsevier, 2021) pp. 195–224.
[48] J. Yu, B. J. Wieder, and C.-X. Liu, Dynamical piezomagnetic effect in time-reversal-invariant weyl semimetals with axionic charge density waves, Physical Review B **104**, 174406 (2021).
[49] F. Wilczek, Two applications of axion electrodynamics, Physical review letters **58**, 1799 (1987).
[50] A. Sekine and K. Nomura, Axion electrodynamics in topological materials, Journal of Applied Physics **129** (2021).
[51] D. M. Nenno, C. A. Garcia, J. Gooth, C. Felser, and P. Narang, Axion physics in condensed-matter systems, Nature Reviews Physics **2**, 682 (2020).
[52] M. De Jong, W. Chen, T. Angsten, A. Jain, R. Notestine, A. Gamst, M. Sluiter, C. Krishna Ande, S. Van Der Zwaag, J. J. Plata, *et al.*, Charting the complete elastic properties of inorganic crystalline compounds, Scientific data **2**, 1 (2015).
[53] X.-X. Dong, J.-X. Chen, Y. Wang, Z.-L. Lv, and H.-Y. Wang, Electronic, elastic and lattice dynamic properties of the topological dirac semimetal na3bi, Materials Research Express **6**, 076308 (2019).
[54] R. Jackiw and C. Rebbi, Solitons with fermion number 1/2, Physical Review D **13**, 3398 (1976).
[55] M. Arai, F. Blaschke, M. Eto, and N. Sakai, Massless bosons on domain walls: Jackiw-rebbi-like mechanism for bosonic fields, Physical Review D **100**, 095014 (2019).
[56] L. Zhang and Q. Niu, Angular momentum of phonons and the einstein–de haas effect, Physical Review Letters **112**, 085503 (2014).
[57] M. Hamada, E. Minamitani, M. Hirayama, and S. Murakami, Phonon angular momentum induced by the temperature gradient, Physical review letters **121**, 175301 (2018).
[58] L.-H. Hu, J. Yu, I. Garate, and C.-X. Liu, Phonon helicity induced by electronic berry curvature in dirac materials, Physical review letters **127**, 125901 (2021).
[59] C.-X. Liu, Probing nieh-yan anomaly through phonon dynamics in the kramers-weyl semimetals of chiral crystals, Physical Review B **106**, 115102 (2022).
[60] H. Zhang, N. Peshcherenko, F. Yang, T. Ward, P. Raghuvanshi, L. Lindsay, C. Felser, Y. Zhang, J.-Q. Yan, and H. Miao, Observation of phonon angular momentum, arXiv preprint arXiv:2409.13462 (2024).
[61] Z. Cheng, R. Li, X. Yan, G. Jernigan, J. Shi, M. E. Liao, N. J. Hines, C. A. Gadre, J. C. Idrobo, E. Lee, *et al.*, Experimental observation of localized interfacial phonon modes, Nature communications **12**, 6901 (2021).
[62] R. Qi, R. Shi, Y. Li, Y. Sun, M. Wu, N. Li, J. Du, K. Liu, C. Chen, J. Chen, *et al.*, Measuring phonon dispersion at an interface, Nature **599**, 399 (2021).
[63] X. Li, B. Fauqué, Z. Zhu, and K. Behnia, Phonon thermal hall effect in strontium titanate, Physical review letters

124, 105901 (2020).
[64] X. Li, Y. Machida, A. Subedi, Z. Zhu, L. Li, and K. Behnia, The phonon thermal hall angle in black phosphorus, Nature Communications **14**, 1027 (2023).
[65] R. Sharma, M. Bagchi, Y. Wang, Y. Ando, and T. Lorenz, Phonon thermal hall effect in charge-compensated topological insulators, Physical Review B **109**, 104304 (2024).
[66] M. M. Otrokov, I. I. Klimovskikh, H. Bentmann, D. Estyunin, A. Zeugner, Z. S. Aliev, S. Gaß, A. Wolter, A. Koroleva, A. M. Shikin, *et al.*, Prediction and observation of an antiferromagnetic topological insulator, Nature **576**, 416 (2019).
[67] D. Zhang, M. Shi, T. Zhu, D. Xing, H. Zhang, and J. Wang, Topological axion states in the magnetic insulator mnbi 2 te 4 with the quantized magnetoelectric effect, Physical review letters **122**, 206401 (2019).
[68] J. Li, Y. Li, S. Du, Z. Wang, B.-L. Gu, S.-C. Zhang, K. He, W. Duan, and Y. Xu, Intrinsic magnetic topological insulators in van der waals layered mnbi2te4-family materials, Science Advances **5**, eaaw5685 (2019).
[69] G. L. Bir and G. E. Pikus, *Symmetry and strain-induced effects in semiconductors* (Wiley, 1974).
[70] R. Winkler, S. Papadakis, E. De Poortere, and M. Shayegan, *Spin-orbit coupling in two-dimensional electron and hole systems*, Vol. 41 (Springer, 2003).
[71] Y. Peter and M. Cardona, *Fundamentals of semiconductors: physics and materials properties* (Springer Science & Business Media, 2010).
[72] E. Witten, Dynamical breaking of supersymmetry, Nuclear Physics B **188**, 513 (1981).
[73] W. Kress and F. W. de Wette, *Surface phonons* (Springer, 1991).
[74] S. M. Girvin and K. Yang, *Modern condensed matter physics* (Cambridge University Press, 2019).